DMD Fast Forward. Published on June 1, 2021 as DOI: 10.1124/dmd.121.000476
This article has not been copyedited and formatted. The final version may differ from this version.

Quantitative investigation of irinotecan metabolism, transport and gut microbiome activation

Md Masud Parvez[1], Abdul Basit[1], Parth B. Jariwala[2], Zsuzsanna Gáborik[3], Emese Kis[3], Scott Heyward[4], Matthew R. Redinbo[2], Bhagwat Prasad[1*]

[1]Department of Pharmaceutical Sciences, Washington State University, Spokane, WA, USA.

[2]Departments of Chemistry, Biochemistry and Microbiology, and the Integrated Program for Biological and Genome Sciences, University of North Carolina at Chapel Hill, Chapel Hill, NC, USA.

[3]SOLVO Biotechnology, Budapest, Hungary

[4]BioIVT Inc., Baltimore, MD, USA.

DMD Fast Forward. Published on June 1, 2021 as DOI: 10.1124/dmd.121.000476
This article has not been copyedited and formatted. The final version may differ from this version.

a) Running title: Disposition mechanisms of irinotecan and its metabolites

b) Corresponding Author: Bhagwat Prasad, Ph.D.

Department of Pharmaceutical Sciences, Washington State University, 412 E Spokane Falls Blvd. Spokane, WA 99202. Email: bhagwat.prasad@wsu.edu. Phone: 509-358-7739

c) The number of tables: 1

The number of figures: 6

The number of references: 59

The number of words in the abstract: 246

The number of in the introduction: 750

The number of words in the discussion: 1500

D) Abbreviation used:

ABC, ATP-binding cassette; AUC, area under the curve; ATP, adenosine 5′-triphosphatedisodium salt; AMP, adenosine 5′-monophosphate monohydrate; BCA, bicinchoninic acid assay; BCRP, breast cancer resistant protein; BSA, bovine serum albumin; CES**,** carboxylesterase; C_{max}, maximum plasma concentration; $CL_{recombinant,}$ recombinant clearance; $CL_{,tissue}$, tissue intrinsic clearance; CL, clearance; CL_{total}, total clearance; DME, drug metabolizing enzyme; DTT, dithiothreitol; DMEM, dulbecco's Modified Eagle medium; $E_{recombinant,}$ enzyme abundance in the recombinant system; $E_{vesicles}$, protein abundance in the vesicles; E_{tissue}, enzyme abundance in the tissue; epiT, epitestosterone; epiTG, epitestosterone glucuronide; f_m, fractional metabolism; f_t, fractional transport; GI, gastrointestinal; HEK-293, human embryonic kidney; IAA, iodoacetamide; IV, intravenous;

DMD Fast Forward. Published on June 1, 2021 as DOI: 10.1124/dmd.121.000476
This article has not been copyedited and formatted. The final version may differ from this version.

K_m, substrate concentration at half-maximum velocity; LFQ, label free quantification; LC-MS/MS, liquid chromatography-tandem mass spectrometry**;** MDCK-II, madin-Darby canine kidney; MRP, multidrug resistance-associated proteins; OATP1B1, organic anion transporting polypeptide-1B1; OATP2B1, organic anion transporting polypeptide-2B1; PBS, phosphate buffer saline; P-gp**,** P-glycoprotein; PK, pharmacokinetic; PBPK, physiologically-based pharmacokinetic modeling; SLC, solute carrier; SN-38-G, SN-38-glucuronide; UGT**,** uridine glucuronosyltransferases; UDPGS, uridine 5′-diphosphoglucuronic acid trisodium salt; V_{max}**,** maximum velocity; v/v, volume/volume;

DMD Fast Forward. Published on June 1, 2021 as DOI: 10.1124/dmd.121.000476
This article has not been copyedited and formatted. The final version may differ from this version.

ABSTRACT

Anticancer drug, irinotecan shows serious dose-limiting gastrointestinal toxicity regardless of intravenous dosing. Although enzymes and transporters involved in irinotecan disposition are known, quantitative contributions of these mechanisms in complex in vivo disposition of irinotecan are poorly understood. We explained intestinal disposition and toxicity of irinotecan by integrating i) in vitro metabolism and transport data of rinotecan and its metabolites, ii) ex vivo gut microbial activation of the toxic metabolite, SN-38, and iii) the tissue protein abundance data of enzymes and transporters relevant to irinotecan and its metabolites. Integration of in vitro kinetics data with the tissue enzyme and transporter abundance predicted that carboxylesterase (CES) mediated hydrolysis of irinotecan is the rate-limiting process in the liver, where the toxic metabolite formed is rapidly deactivated by glucuronidation. In contrast, the poor SN-38 glucuronidation rate as compared to its efficient formation by CES2 in the enterocytes is the key mechanism of the intestinal accumulation of the toxic metabolite. The biliary efflux and OATP2B1 mediated enterocyte uptake can also synergize buildup of SN-38 in the enterocytes, whereas intestinal P-glycoprotein (P-gp) likely facilitates SN38 detoxification in the enterocytes. The higher SN-38 concentration in the intestine can be further nourished by β-d-glucuronidases. Understanding the quantitative significance of the key metabolism and transport processes of irinotecan and its metabolites can be leveraged to alleviate its intestinal side effects. Further, the proteomics-informed quantitative approach to determine intracellular disposition can be extended to determine susceptibility of cancer cells over normal cells for precision irinotecan therapy.

DMD Fast Forward. Published on June 1, 2021 as DOI: 10.1124/dmd.121.000476
This article has not been copyedited and formatted. The final version may differ from this version.

Significance Statement

This work provides a deeper insight into the quantitative relevance of irinotecan hydrolysis (activation), conjugation (deactivation), and deconjugation (reactivation) by human or gut microbial enzymes or transporters. The results of this study explain the characteristic intestinal exposure and toxicity of irinotecan. Quantitative tissue-specific in vitro to in vivo extrapolation approach presented in this study can be extended to cancer cells.

DMD Fast Forward. Published on June 1, 2021 as DOI: 10.1124/dmd.121.000476
This article has not been copyedited and formatted. The final version may differ from this version.

1. INTRODUCTION

Unpredictable safety and efficacy of investigational drugs has replaced poor pharmacokinetics (PK) as the primary reason for drug attrition during clinical development (Kola and Landis, 2004; Hay *et al.*, 2014). Poor drug safety is associated with nearly 40% attrition during drug development (Waring *et al.*, 2015). Likewise, *in silico* pharmacophore modeling to predict drug potency (efficacy or toxicity) are not accurate because they solely rely on the physicochemical properties of a drug compound and ignore drug concentration at site of action (Sliwoski *et al.*, 2013). The target-site drug concentration depends on a complex interplay of multiple drug-related and physiological factors such as the activity of transporters and drug metabolizing enzymes (Bhatt *et al.*, 2019). For example, decreased P-glycoprotein (P-gp) mediated efflux is associated with the accumulation and dendritic spine injury of 8-hydroxy metabolite of efavirenz (Tovar-y-Romo *et al.*, 2012). Other examples influenced by the enzymatic activation or transporters cause kidney toxicity of the antiviral drugs, tenofovir, and cidofovir (Zhang *et al.*, 2015). Further, enterohepatic recycling of drugs and metabolites involving drug transport and gut microbial metabolisms also impacts intestinal exposure and systemic half-life of drugs (Sun *et al.*, 2019). Therefore, a systems level understanding of the interplay between intracellular and systemic drug disposition processes is crucial for an accurate prediction of target-site exposure, efficacy, and safety of drugs that undergo complex disposition. A widely used topoisomerase I inhibitor and colorectal and pancreas cancer prodrug, irinotecan (Gilbert *et al.*, 2012), is one such drug which causes dose-limiting gastrointestinal (GI) toxicity after an intravenous (IV) dose.

Irinotecan is given as a prodrug due to its better solubility for IV administration and to avoid high systemic exposure of the toxic metabolite, SN38 (Hageman and Morozowich, 2007). After IV irinotecan dose, cholinergic diarrhea occurs immediately, which is followed by a late onset severe diarrhea due to the direct toxicity in GI mucosa that is also influenced by GI dysmotility. In particular, irinotecan induces apoptosis and hyperproliferation in both the small and the large intestine in the later stages (Gibson and Keefe, 2006). Although the GI

DMD Fast Forward. Published on June 1, 2021 as DOI: 10.1124/dmd.121.000476
This article has not been copyedited and formatted. The final version may differ from this version.

toxicity is linked to the metabolism and transport of irinotecan, (Di Martino *et al.*, 2011; Chen *et al.*, 2013; Teft *et al.*, 2015) the preferential toxicity in the intestinal mucosa is not well understood. For example, carboxylesterase (CESs) and uridine glucuronosyltransferases (UGTs) are known enzymes responsible for irinotecan to SN-38 (active and toxic metabolite) (Pommier, 2006; Rivory and Robert, 1995) and SN-38 to SN-38-glucuronide (SN-38-G) conversion in the liver and intestine (Ando *et al.*, 2000; Hanioka *et al.*, 2001; Jinno *et al.*, 2003). Similarly, some membrane transporters also contribute significantly to the disposition and tissue distribution of irinotecan (Nakatomi *et al.*, 2001; Lalloo *et al.*, 2004; Nozawa *et al.*, 2005; Fujita *et al.*, 2016) and the conversion of SN-38-G to SN-38 by gut microbial β-glucuronidase (GUS) has shown to be associated with the dose-limiting GI toxicity (Bhatt *et al.*, 2020). But to what extent individual disposition processes contribute to irinotecan and SN-38 disposition in the intestine is not well characterized. To fill this knowledge gap, we hypothesized that integration of the in vitro metabolism and transport data of irinotecan and its metabolites with quantitative abundance of individual enzymes and transporters in each organ can explain tissue-specific exposure of its toxic metabolite, SN-38.

We estimated the quantitative contributions of metabolism and transport pathways involved in irinotecan intestinal exposure. First, we determined the in vitro kinetics parameters of metabolism, uptake and efflux transport of irinotecan and its metabolites. These data were then normalized by the tissue specific protein abundance of the enzymes and transporters to estimate individual contributions of these processes in irinotecan disposition in human intestine, liver, and kidney. In addition, we investigated SN-38 reactivation by gut microbial β-glucuronidases in human fecal homogenates using a previously established chemoproteomics strategy (Jariwala *et al.*, 2020). By integrating these data, we answered **a)** why does irinotecan show high intestinal exposure and GI specific toxicity after intravenous dose, and **b)** why do irinotecan and SN-38 mainly eliminated in the feces but the SN-38-G is excreted mainly in the urine (Slatter *et al.*, 2000).

DMD Fast Forward. Published on June 1, 2021 as DOI: 10.1124/dmd.121.000476
This article has not been copyedited and formatted. The final version may differ from this version.

Although in vivo imaging and *in vitro* approaches have been used to estimate tissue drug concentrations (Mateus *et al.*, 2017; Guo *et al.*, 2018), these models do not provide mechanistic information regarding multiple factors linking host enzymes-transporters and the gut microbiota. The novel quantitative approach developed here can be applied to predict tissue exposure and toxicity of drugs undergoing multi-process disposition, e.g., enterohepatic recirculation, transporter-enzyme interplay, and the gut microbiome contribution.

2. MATERIALS AND METHODS

2.1 Materials

Irinotecan, SN-38, and SN-38-G were purchased from PerkinElmer (Waltham, MA, USA). Bovine serum albumin (BSA), dithiothreitol (DTT), iodoacetamide (IAA), and trypsin protease (mass-spectroscopy grade), phosphate-buffered saline (PBS) and Hank's balanced salt solution (HBSS), hepatocyte maintenance supplement pack (Serum-free), membrane protein extraction kit (Mem-PER Plus kit), and bicinchoninic acid assay (BCA) kit were purchased from Thermo Fisher Scientific (Rockford, IL). Recombinant UGT and CES enzymes were procured from Corning (Riverfront, NY). Human liver S9 (pool of n = 10) and intestinal S9 (pool of n = 15) fractions were purchased from Sekisui XenoTech LLC (Kansas City, KS). Membrane vesicle (MV) or cell-lines overexpressing P-gp, breast cancer resistant protein (BCRP), multidrug resistance-associated proteins (MRP2, MRP3, and MRP4), organic anion transporting polypeptide (OATP1B1 and OATP2B1) transporters were provided by Solvo Biotechnology (Budapest, Hungary). The multiscreen^{TM} HTS Vacuum Manifold and 96-well filter plates with class B glass fiber filters were obtained from EMD Millipore (Billerica, MA). Dulbecco's Modified Eagle medium (DMEM), penicillin-streptomycin, alamethicin, uridine 5′-diphosphoglucuronic acid trisodium salt (UDPGA), adenosine 5′-triphosphate (ATP) disodium salt, adenosine 5′-monophosphate (AMP) monohydrate, magnesium chloride ($MgCl_2$), glutathione, tris [hydroxymethyl] aminomethane (Tris-Base), NaCl, sucrose, 3-[N-

DMD Fast Forward. Published on June 1, 2021 as DOI: 10.1124/dmd.121.000476
This article has not been copyedited and formatted. The final version may differ from this version.

morpholino] propanesulfonic acid (MOPS), epitestosterone, and epitestosterone glucuronide were purchased from Sigma Aldrich (St. Louis, MO). Poly-D-lysin coated 24-well tissue culture plates were from BD biosciences, (Franklin Lakes, NJ). Stable isotope-labeled (heavy) peptides and synthetic unlabeled (light) peptides for targeted proteomics assay were purchased from Thermo Fisher Scientific (Rockford, IL) and New England Peptides (Boston, MA), respectively. All other reagents and chemicals were purchased from commercial suppliers offering the highest purity.

2.2. Outline of experimental workflow

A systematic workflow used for the quantitative characterization of irinotecan disposition involved the following five steps **(Figure S1)**.

I. Determination of the metabolic intrinsic clearance of irinotecan and SN-38 by recombinant CESs and UGTs, respectively.
II. Confirmation of the rate-determining steps in irinotecan metabolism in S9 fractions and hepatocytes.
III. Determination of the uptake and efflux transport intrinsic clearance of irinotecan, SN-38, and SN-38-G using *in vitro* cellular uptake or vesicular assay.
IV. Estimation of the relative contributions of individual enzymes and transporters (fractional metabolism, f_m and fractional transport, f_t) by quantifying and comparing the protein abundance data in *in vitro* systems versus liver, intestine, and kidney tissues.
V. Investigation of SN-38 reactivation by gut bacterial β-glucuronidases in human fecal homogenate.

2.1 Irinotecan and SN-38 metabolism in recombinant enzymes, S9 fractions and hepatocytes

DMD Fast Forward. Published on June 1, 2021 as DOI: 10.1124/dmd.121.000476
This article has not been copyedited and formatted. The final version may differ from this version.

Metabolic intrinsic clearances of irinotecan and SN-38 were determined by incubation in individual recombinant enzymes using an established method (Hanioka *et al.*, 2001). Sequential metabolism of irinotecan in human liver and intestinal S9 fractions was investigated as done previously (Zhang *et al.*, 2018). The relative contributions of CESs and UGTs on irinotecan and SN-38 metabolism were characterized in cryopreserved individual human hepatocytes (n = 3 donors) (Lau *et al.*, 2002). Briefly, the potential of irinotecan metabolism by CES1 and CES2 was estimated by incubating irinotecan (5 and 10 µM) with 10 µg of recombinant CES1 and CES2 in 50 mM Tris buffer (pH 7.0) in 100 µL incubation volume. The reaction was performed for 15 minutes at 37 °C with gentle shaking and quenched by the addition of ice-cold 200 µL of 1:1 acetonitrile: formic acid (0.2%) containing internal standard (10 ng/mL epitestosterone). The reaction mix was centrifuged at 10000 x g for 5 minutes at 4 °C to remove the cell debris and the supernatant was collected to quantify the metabolite formation by LC-MS/MS. Since the screening assay indicated the involvement of CES1 and CES2 in irinotecan hydrolysis, a detailed irinotecan metabolism kinetics assay was performed following the same protocol across a wide concentration range, 1 - 400 µM. SN-38 formation was monitored in the incubation buffer to estimate the non-enzymatic hydrolysis of irinotecan.

SN-38 (5 and 10 µM) was incubated with recombinant UGT1A1, UGT1A4, UGT1A6, UGT1A9, UGT2B7, UGT2B15, and UGT2B17 enzymes (20 µg per reaction) to identify UGTs involved in SN-38 glucuronidation. The assay was performed at pH 7.4 in 100 µL of buffer consisted of 5 mM $MgCl_2$, 100 mM KPO_4, alamethicin (0.2 mg/mL, final concentration), and BSA (0.2%). After addition of the substrate and the enzyme, the buffer system was pre-incubated on ice for 15 minutes to allow microsomal pore formation by alamethicin. The glucuronidation was initiated by adding 2.5 mM UDPGA. After 30 minute incubation at 37 °C with gentle shaking, the reaction was stopped by addition 200 µl ice-cold acetonitrile:0.2% formic acid (1:1; volume:volume) containing internal standard (10 ng/mL epitestosterone glucuronide). In parallel, the reaction was also performed in the absence of UDPGA (negative control). The reaction mix was centrifuged at 10000 x g for 5 minutes at 4 °C to

DMD Fast Forward. Published on June 1, 2021 as DOI: 10.1124/dmd.121.000476
This article has not been copyedited and formatted. The final version may differ from this version.

remove precipitated proteins and the supernatant was collected to quantify the metabolite formed. The metabolism kinetic experiment was conducted for the shortlisted UGTs. Briefly, SN-38 was incubated across 1-120 µM concentration range with and without UDPGA using the protocol described above. All reactions were carried out in triplicates. The concentration-dependent SN-38 and SN-38-G formation were measured by a validated LC-MS/MS method (Table S1). The maximum velocity (V_{max}) and the substrate concentration at half-maximum velocity (K_m) were estimated, and the V_{max} was normalized by tissue enzyme abundance (pmol/mg of total protein) (**Table S2**).

Irinotecan (1-400 µM) and SN-38 (1-120 µM) were incubated with the human liver (a pool of n = 10) and intestinal (a pool of n = 15) S9 fractions (20 µg per reaction). UDPGA (2.5 mM) was added to the SN-38 metabolism reaction and incubated for 30 minutes in a buffer containing 5 mM $MgCl_2$, 100 mM KH_2PO_4, alamethicin (0.2 mg/mL), and BSA (0.2%) at pH 7.4. The metabolism was quenched by addition of 200 µL ice-cold 1:1 acetonitrile:0.2% formic acid containing corresponding epitestosterone (epiT) and epitestosterone glucuronide (epiTG) (i.e., the internal standards for SN-38 and SN-38-G, respectively). The reaction mix was centrifuged at 10000 x g for 5 minutes at 4 $^{\circ}$C to remove the precipitated proteins. The supernatant was subjected to metabolite quantification by LC-MS/MS (**Table S2**).

The liver and intestinal S9 fraction incubations were performed to quantify the sequential formation of SN-38 and SN-38-G by CESs and by UGTs, respectively. Briefly, irinotecan (1-400 µM) was incubated for 30 minutes with the liver and intestinal S9 fractions (20 µg/reaction) with and without 2.5 mM UDPGA in triplicates using the protocol described above. The reaction was quenched, and irinotecan, SN-38 and SN-38-G were quantified by LC-MS/MS (Table S1). The rate of metabolite formation was estimated and normalized by the tissue protein abundance (pmol/ mg of S9 protein).

For irinotecan and SN38 metabolism in human hepatocytes, the cryopreserved cells were thawed at 37°C in a water-bath and transferred to a 50-mL tube containing 15 mL of suspension medium at 4°C. The cells were centrifuged at 600 rpm at 4°C for 5 minutes and

DMD Fast Forward. Published on June 1, 2021 as DOI: 10.1124/dmd.121.000476
This article has not been copyedited and formatted. The final version may differ from this version.

washed twice. The pellet was gently resuspended in the medium to a final density of 2 million cells/mL. The viability of individual hepatocyte lots was determined by trypan blue staining method immediately after thawing and centrifugation. Both irinotecan and SN-38 were tested at 1, 10 and 100 µM final concentrations. The incubations were carried out with 0.5 x 10^6 hepatocytes/mL in 96-well plates at 37°C for 30 minutes. The reaction was stopped by the addition of 200 µL ice-cold 1:1 acetonitrile:0.2% formic acid containing epitestosterone and epitestosterone glucuronide (internal standards for SN-38 and SN-38-G, respectively) and the samples were centrifuged to collect the supernatants for LC-MS/MS analysis of irinotecan, SN-38 and SN-38-G (Table S1). UGT and CES enzymes were quantified in the same hepatocytes using method described below.

2.2 Cellular and vesicular uptake transport assay of irinotecan, SN-38 and SN-38-G

First, active uptake of irinotecan, SN-38 and SN-38-G by hepatic and intestinal OATP transporters was investigated using a cellular transport assay as described previously (Izumi *et al.*, 2015). We used HEK-293 and MDCK-II cells stably expressed OATP1B1 and OATP2B1, respectively. Briefly, transporter or mock-transfected HEK293 and MDCKII cells were grown in tissue culture flasks at 37 ^{o}C in Dulbecco's modified Eagle medium (DMEM) supplemented with 10% fetal bovine serum, 1% nonessential amino acids, 2 mM L-glutamine and 100 U/mL penicillin-streptomycin supplemented with 5% CO_2 and 3 µg/mL puromycin. Approximately 4 x 10^5 cells were seeded per well in a poly-D-lysine-coated 24-well plate. After 24 hrs, five mM sodium butyrate was added to the cells for another 24 hours to induce OATP expression. Cells were washed twice with 1X PBS and pre-incubated with 300 µl HBSS for 10 minutes at 37 °C before incubation with medium containing irinotecan, SN-38 and SN-38-G for 5 minutes. Cells were washed three times with ice-cold 1X PBS and the cell pellet was lysed by adding acetonitrile containing the internal standards (epitestosterone for irinotecan and SN-38, epitestosterone glucuronide for SN-38-G). Cell

DMD Fast Forward. Published on June 1, 2021 as DOI: 10.1124/dmd.121.000476
This article has not been copyedited and formatted. The final version may differ from this version.

lysate was centrifuged at 10000 x g for 10 minutes and the supernatant was subjected to LC-MS/MS analysis. SN-38 and SN-38-G transport kinetics experiments were conducted for the shortlisted transporters (final concentrations, 1 to 200 µM). Further, total protein quantification was performed by BCA assay and transporter quantification by LC-MS/MS quantitative proteomics. K_m and V_{max} were calculated, and the V_{max} was normalized by the transporter protein abundance in the cell system. Second, we characterized the role of hepatic and intestinal efflux transporters (P-gp, BCRP and MRPs) in the transport of irinotecan and its metabolites by vesicular uptake assay using ABC efflux transporter-expressing MVs (Li *et al.*, 2019). The MVs were diluted in the transport buffer (40 mM MOPS-Tris (pH 7.0), 70 mM KCl, and 7.5 mM $MgCl_2$ for MRP2-vesicles, and 10 mM Tris-HCl, 10 mM MgCl2, and 250 mM sucrose for BCRP, MDR1, MRP3 and MRP4-vesicles) and added (50 µL/well) to a 96-well plate on ice. The transport of irinotecan, SN-38 and SN-38-G (1 µM) was initiated by adding 25 µL AMP or ATP (4 mM) at 37°C for 20 (irinotecan and SN-38) or 30 seconds (SN-38-G). The reaction was stopped by the addition of 200 µL ice-cold washing buffer (40 mM MOPS-Tris, pH 7.0, 70 mM KCl), which was washed for 5 times with 200 µL of ice-cold wash buffer. The MVs were eluted with 100 µL of 1:1 acetonitrile:0.2% formic acid containing corresponding deuterated internal standards and kept 1 hour at room temperature for vesicle lysis. The lysed vesicles containing substrates were collected through the vacuum filtration into a 96-well collector plate. The plate was centrifuged at 3000 xg for 2 minutes to collect the supernatant and subjected to substrate quantification by LC-MS/MS. Transport kinetics data were obtained for the shortlisted transporters with a concentration range (1 to 200 µM). Transport kinetic parameters (V_{max} and K_m) were estimated and normalized by the protein abundance (pmol/ mg of total protein) in the *in vitro* system.

2.3 Quantification of CESs, UGTs, and transporter proteins

DMD Fast Forward. Published on June 1, 2021 as DOI: 10.1124/dmd.121.000476
This article has not been copyedited and formatted. The final version may differ from this version.

The protein abundance of enzymes and transporters was quantified in the recombinant systems, S9 fractions, transporter-expressed cell system, cryopreserved hepatocytes, and tissues (liver, intestine, kidney, lung) using optimized LC-MS/MS methods **(Table S1)** (Xu *et al.*, 2017). The crude membranes were isolated from the cell pellets using a membrane protein extraction kit (Thermo Fisher Scientific, Rockford, IL). Approximately 10 million cells were suspended with the permeabilization buffer (250 µL) and gently mixed and kept on a compact digital waving rotator (Thermo Fisher Scientific, Rockford, IL) for 30 minutes (4°C) at 300 rpm. The permeabilized cell suspension was centrifuged at 16000 x g for 15 minutes (4°C). The pellet was resuspended with solubilization buffer (250 µL), gently mixed, incubated for 60 minutes at 300 rpm (4°C), and centrifuged at 16,000 x g for 15 minutes (4°C). The supernatant containing membrane proteins was collected and the total protein concentration was measured by BCA assay. Eighty µL of 2 mg/mL protein sample was mixed with 30 µL ammonium bicarbonate buffer (100 mM, pH 7.8), 10 µL dithiothreitol (250 mM), 20 µL BSA (0.02 mg/mL), followed by heat denaturation and 10 minutes reduction at 95 °C. Ten µL of iodoacetamide (100 mM) was added after cooling at room temperature and kept in dark for 30 minutes. Ice-cold acetone (500 µL) was added to the sample, which was kept at -20 °C for 30 minutes before centrifugation at 16000 x g for 5 minutes at 4°C. Protein pellet was washed with 500 µL methanol and the sample was centrifuged at 8000 x g for 5 minutes at 4°C and the pellet was collected after air drying. The pellet was resuspended with 60 µL ammonium bicarbonate (50 mM, pH 7.8) and 20 µL trypsin (0.16 µg/µL) for 16 hours at 300 rpm (37 °C). Trypsin digestion was quenched on ice with addition of 20 µL of stable isotope labeled peptide cocktail (internal standard) and 10 µL acetonitrile: water 80:20 (v/v) with 0.5% formic acid. The sample was prepared by centrifuging at 8000 x g for 5 minutes (4 °C), and the supernatants (50 µL) were subjected to LC-MS/MS quantifications. Previously characterized pooled human liver microsome and liver membrane samples were digested and used as calibrators for the quantification of enzymes and transporters, respectively (Zhang *et al.*, 2018).

DMD Fast Forward. Published on June 1, 2021 as DOI: 10.1124/dmd.121.000476
This article has not been copyedited and formatted. The final version may differ from this version.

2.4 SN-38-G to SN-38 reactivation by gut bacterial β-d-glucuronidase in human fecal samples

Human fecal samples were collected and stored at –80°C until further use. Characterization of the bacterial flora and ethical concerns was previously reported by us, where the total fecal protein was extracted (Jariwala *et al.*, 2020) to quantify SN-38 reactivation rate by the bacterial β-d-glucuronidase. In brief, approximately 5 gram of thawed fecal material in a solution containing 25 mL of cold extraction buffer (pH 6.5, 25 mM HEPES, 25 mM NaCl with Roche cOmplete^{TM} protease inhibitor cocktail) and 500 mg of autoclaved garnet beads was vortexed vigorously to break up dense, fibrous material. The suspended sample was centrifuged at low speed (300 x g, 5 min., 4 °C) to separate out any insoluble fecal material. After decanting the microbial supernatant from the fecal homogenate, an additional 25 mL of cold extraction buffer was added to the remaining fibrous material and the extraction process was repeated. The combined microbial supernatant (~40–45 mL) was centrifuged at low speed to remove any remaining insoluble debris. This process was repeated with the decanted microbial supernatant. The microbial supernatant was ultrasonicated for 1.5 minutes while on ice. The lysate was mixed by inversion and the sonication repeated. The lysed cells were centrifuged at high speed (17,000 x g, 20 min., 4°C) to remove cellular debris. The decanted lysate was concentrated, and metabolites were removed by buffer exchanging with fresh extraction buffer. The concentration of total protein in the fecal extract was calculated using a standard Bradford Assay protocol. The human fecal extract was aliquoted and snap frozen using liquid nitrogen. The aliquots were stored at –80°C until further use. Relative quantifications of bacterial β-d-glucuronidase enzymes from the fecal extracts were obtained following a previously described protocol (Jariwala *et al.*, 2020). Relative quantification values were reported as label free quantification (LFQ) intensities,

DMD Fast Forward. Published on June 1, 2021 as DOI: 10.1124/dmd.121.000476
This article has not been copyedited and formatted. The final version may differ from this version.

which were normalized, and combined peptide signal intensities as determined by the MaxLFQ algorithm in MaxQuant (Jariwala *et al.*, 2020).

2.5 Data analysis of drug metabolism, transport, and microbial re-activation

Irinotecan and SN-38 metabolite formation kinetic parameters were estimated by fitting the Michaelis-Menten equation (Eq. 1) in GraphPad Prism (ver. 5.0) (La Jolla, CA).

$$Y = (V_{max} \times S) / (K_m + S) \quad \textbf{(1)}$$

Where, Y is the metabolite formation rate of SN-38 and SN-38-G (pmol/min/pmol of protein), S is the substrate concentration in the reaction (μM), K_m is the Michaelis-Menten constant (μM) and V_{max} is the maximum rate. The metabolism rate was normalized by the enzyme abundance in the recombinant versus human tissues (liver, intestine, and kidney). To address the non-enzymatic degradation, SN-38 formation was subtracted from the value in the incubation buffer. The vesicular and cellular uptake kinetic parameters were estimated using Michaelis-Menten equation (Eq. 1) after subtracting the passive uptake in the mock-transfected system. Transport data were normalized by the protein abundance value (pmol per mg protein). The % of inside-out data of the MVs from our previous study (Li *et al.*, 2019) was used to normalize the transport kinetic parameters.

Two-sided Student's *t*-test was used to determine the statistical significance of the differences between the control (e.g., mock transfected cells, vesicles, or without UDPGA incubations) verses metabolism/transport data in recombinant systems and with cofactors. The results are expressed as mean ± SD. The Pearson correlation between SN-38-G deglucuronidation and β-glucuronidase (LFQ) was obtained using GraphPad Prism (ver. 5.0). P value <0.05 was considered statistically significant.

2.6 *In vitro* to *in vivo* scaling of fractional contribution of individual enzyme and transporter

DMD Fast Forward. Published on June 1, 2021 as DOI: 10.1124/dmd.121.000476
This article has not been copyedited and formatted. The final version may differ from this version.

A summary of stepwise scaling approach to determine fractional contributions of individual enzymes and transporters in irinotecan disposition is provided below and elaborated in **Supporting information**.

1. The CES and UGT mediated intrinsic clearance (CL) data were normalized by the abundance of individual enzymes in the recombinant system (Eq. 2).

$CL_{recombinant} = V_{max}/K_m \times E_{recombinant}$ **(2)**

Where, $E_{recombinant}$ is the enzyme abundance in the recombinant system **(Table S2).**

2. The tissue intrinsic clearance ($CL_{,tissue}$) of individual enzymes in whole organ was estimated using Eq. 3.

$CL_{,tissue} = CL_{recombinant} \times E_{tissue}$ **(3)**

3. The tissue intrinsic clearance for CES or UGT was used to calculate the total intrinsic clearance using Eqs. 4 and 5.

$CL_{total,CES\ (SN\text{-}38)} = CL_{CES1} + CL_{CES2}$ **(4)**

$CL_{total,UGT\ (SN\text{-}38\text{-}G)} = CL_{UGT1A1} + CL_{UGT1A6} + CL_{UGT1A9} + CL_{UGT2B15}$ **(5)**

4. The scaled total clearance allowed the calculation of fractional metabolism (f_m) of irinotecan and SN-38 by individual CES and UGT *in vivo* using Eq. 6

$f_m = CL_{I,DME} / CL_{total}$ **(6)**

$CL_{I,DME}$ is the tissue intrinsic clearance of individual enzymes

Similarly, *in vitro* transport kinetics were used to estimate the fractional contribution (f_t) of each transporter (Li *et al.*, 2019), where the intrinsic clearance for vesicular uptake was calculated using *in vitro* transport kinetics data normalized by % of inside-out of the transporters in the vesicular system (Eq. 7).

$CL_{int,\ vesicles} = (V_{max,vesicles}/K_{m,\ vesicles}) \times 1/E_{vesicles} \times \%\ inside\text{-}out$ **(7)**

DMD Fast Forward. Published on June 1, 2021 as DOI: 10.1124/dmd.121.000476
This article has not been copyedited and formatted. The final version may differ from this version.

The vesicular and cellular intrinsic clearance was scaled to tissue intrinsic CL using transporter expression data, where, f_t was estimated similar to approaches described for metabolism using Eq. 8-13

$$CL = CL_{int,vesicles} \times E_{tissue,total} \quad \textbf{(8)}$$

$$CL_{total,ABC,(irino)} = CL_{P\text{-}gp} + CL_{MRP2} + CL_{BCRP} \quad \textbf{(9)}$$

$$CL_{total,ABC,(SN\text{-}38)} = CL_{P\text{-}gp} + CL_{BCRP} \quad \textbf{(10)}$$

$$CL_{total,SLC,(SN\text{-}38)} = CL_{OATP1B1} + CL_{OATP2B1} \quad \textbf{(11)}$$

$$CL_{total,ABC,(SN\text{-}38\text{-}G)} = CL_{MRP2} + CL_{MRP3} + CL_{BCRP} \quad \textbf{(12)}$$

$$f_t = CL_{I,transporter} / CL_{total} \quad \textbf{(13)}$$

Where, $CL_{I,transporter}$ is the tissue intrinsic clearance of individual transporters.

3. RESULT

3.1 Irinotecan and SN-38 metabolism by recombinant CES and UGT enzymes

CES2 hydrolyzed irinotecan to SN-38 more efficiently than CES1 **(Figure S2**). Non-enzymatic hydrolysis of irinotecan to SN-38 was also observed, which was subtracted prior to enzyme kinetics estimation. The kinetics assay confirmed ~7-fold higher intrinsic clearance of CES2 than CES1 **(Figure 1A and Table 1).** In particular, CES2 showed ~2-fold lower affinity (2-fold higher K_m) and 11-fold greater capacity (V_{max}) for irinotecan hydrolysis consistent with literature (Humerickhouse *et al.*, 2000) **(Table 1).** However, overall slower rate of CES-mediated irinotecan hydrolysis to SN-38 was consistent as reported for other exogenous compound such as mycophenolate mofetil (Fujiyama *et al.*, 2010), procaine and ACE inhibitors (Di, 2019).

Likewise, the initial screening assay identified that SN-38 is glucuronidated to SN-38-G by UGT1A1, 1A6, 1A9 and 2B15 **(Figure S2).** According to the kinetics assay, UGT1A1 was confirmed to be the high-capacity enzyme for SN-38 glucuronidation with >20-fold higher

DMD Fast Forward. Published on June 1, 2021 as DOI: 10.1124/dmd.121.000476
This article has not been copyedited and formatted. The final version may differ from this version.

V_{max} compared to other UGTs (**Figure 1B, Table 1**). The affinity of SN-38 towards UGTs was similar across UGT1A1, UGT1A6, and UGT1A9, but it was ~5-fold lower for UGT2B15 **(Table 1)**.

3.2 Irinotecan and SN-38 metabolism in human tissue S9 fractions

SN-38 formation rate was 3-fold higher in the intestinal S9 fraction than in the liver S9, however, SN-38-G formation rate was 3-fold lower in the intestinal S9 **(Figure 2A).** The quantification of metabolite formation rates across different concentrations (3-400 µM) in S9 fractions revealed 6-fold higher SN-38-G levels as compared to SN-38 in the liver. In contrast, SN-38 to SN-38-G ratio was 3-fold in the intestine **(Figure 2A).** The direct incubation of SN-38 in S9 fractions in the presence of UDPGA showed 3-fold greater SN-38-G formation rate in the liver than in the intestine **(Figure 2B)**. Likewise, the percent of unmetabolized SN-38 was 3-fold lower in the liver than in the intestinal S9 **(Figure S4)**. When SN38 was directly incubated in the S9 fractions, the ratio of SN-38 and SN-38-G formation was significantly lower in the liver and compared to the intestine **(Figure 2C)**, whereas significantly higher SN-38-G formation was observed in the liver **(Figure 2D)** as compared to the intestine.

3.3 Irinotecan and SN-38 metabolism in cryopreserved human hepatocytes

Irinotecan and SN-38 metabolism in human hepatocytes (n=3) was in line to that in the recombinant and the S9 fraction data **(Figure S5)**. The sequential metabolism of irinotecan showed significantly slower SN-38-G formation rate than the direct metabolism of SN-38 to SN-38-G. Similarly, SN-38 to irinotecan ratio was significantly lower than SN-38-G to SN-38 ratio in the human hepatocytes **(Figure 2E and 2F).** While CES-mediated hydrolysis was linear with the concentration, UGT mediated SN-38-G formation was saturable at higher concentrations **(Figure 2G)**.

DMD Fast Forward. Published on June 1, 2021 as DOI: 10.1124/dmd.121.000476
This article has not been copyedited and formatted. The final version may differ from this version.

3.4 Vesicular transporter uptake of irinotecan, SN-38 and SN-38-G

Irinotecan, SN-38 and SN-38-G are actively transported by P-gp, MRP2 and BCRP. In addition, SN-38 and SN-38-G are also transported by MRP3. None of these compounds were substrates of MRP4 **(Figure S3).** Irinotecan showed highest affinity for P-gp followed by BCRP > MRP2 (**Table 1).** However, the protein-normalized intrinsic clearance of irinotecan transport (CL) was highest for BCRP than P-gp > MRP2. BCRP showed highest transport efficiency for SN-38 and SN-38-G (**Figure 3A to 3C).** P-gp showed ~2-fold greater affinity and ~25-fold higher CL for irinotecan as compared to MRP2, whereas irinotecan CL by P-gp did not differ from that of BCRP (**Table 1**). P-gp and BCRP showed similar affinity for SN-38, but BCRP mediated efflux was ~2-fold greater (**Table 1**). BCRP mediated CL was >70-fold higher for SN-38-G as compared to that by MRPs (**Table 1**).

3.5 OATP mediated transport of irinotecan, SN-38, and SN-38-G

Irinotecan was not actively transported by OATP1B1 and OATP2B1 expressing cells, but SN-38 showed significant uptake by OATP1B1 and OATP2B1 as compared to the mock-control cells **(Figure 3).** OATP1B1 mediated hepatic uptake of SN-38 showed significantly lower affinity (66-fold higher K_m) and high capacity (300-fold high V_{max}) as compared to OATP2B1 **(Figure 3D to 3F, and Table 1).**

3.6 Fractional contributions of individual enzymes (f_m) and transporters (f_t) to irinotecan disposition

Although CES2 is the major enzyme in the metabolism of irinotecan to SN-38 in vitro using the recombinant system, after normalization by the tissue abundance of CES enzymes, the estimated f_m of CES1 and CES2 in the liver in irinotecan hydrolysis was comparable (53% and 47%, respectively). CES1 levels were 65-fold lower in the intestine, and hence CES2

DMD Fast Forward. Published on June 1, 2021 as DOI: 10.1124/dmd.121.000476
This article has not been copyedited and formatted. The final version may differ from this version.

was the primary intestinal esterase for irinotecan hydrolysis **(Figure 4A, Table S3)**. UGT-mediated SN-38-G formation was primarily mediated by UGT1A1 with small contributions of UGT1A9, UGT1A6, and UGT2B15. After normalizing with the tissue UGT abundance data, the hepatic f_m value of UGTs were in the following order: UGT1A1 >> UGT1A9 > UGT2B15 > UGT1A6 (0.62:0.31:0.06:0.02) **(Figure 4B, Table S4)**. In the intestine, UGT1A1 was the only enzyme responsible for SN-38-G clearance (**Figure S2**), whereas UGT1A9 was estimated to play predominant role in SN-38-G formation in the kidney (f_m = 0.98) **(Figure 4B)**.

The f_t values of different efflux transporters in irinotecan transport were in the following order P-gp >> BCRP > MRP2, irrespective of the organs (liver, intestine, or kidney) **(Figure 4C, Table S5)**. The P-gp and BCRP mediated biliary efflux of SN-38 was comparable, whereas 90% of SN-38 was transported by P-gp in the kidney **(Figure 4D)**. BCRP was the predominant transporter for SN-38-G with f_t value of 60-80% in the liver, intestine, and kidney, however, MRP3 was the sole contributor in SN-38-G efflux into the blood from the liver and enterocytes **(Figure 4E, Table S6)**. OATP1B1 was the predominant player in SN-38 and SN-38-G uptake into the liver, whereas, OATP2B1 was solely responsible for SN-38 uptake in the intestine **(Figure 4F)**.

3.7 SN-38-G to SN-38 reactivation by gut bacterial β-glucuronidase activity in human fecal samples

SN-38 incubation in the human fecal samples (n=7) showed significant β-glucuronidase mediated SN-38-G reactivation to SN-38. The rate of SN-38 formation was variable by 4-fold between samples (**Figure 5A**). Total β-glucuronidase protein levels were measured by an activity-based probe-enabled proteomics pipeline as described (Jariwala *et al.*, 2020). LFQ values of β-glucuronidase protein levels were correlated with SN-38 reactivation rate (Pearson R = 0.89) (**Figure 5B**).

DMD Fast Forward. Published on June 1, 2021 as DOI: 10.1124/dmd.121.000476
This article has not been copyedited and formatted. The final version may differ from this version.

DISCUSSION

Current *in vitro* and preclinical drug toxicity data often fail to predict drug safety in humans. The lack of an in vitro or preclinical approach for estimating tissue drug concentration is one of the major reasons for unpredictable toxicity. The tissue drug concentration often depends on complex interplay between drug metabolism and transport processes. Furthermore, not only the host mechanisms, the gut microbial processing can also influence intestinal exposure, clinical PK (Sharma *et al.*, 2019), efficacy and safety of drugs (Li *et al.*, 2016).

We explained the intestinal exposure and irinotecan toxicity by integrating in vitro data with tissue specific abundance of enzymes and transporters, and ex vivo gut microbiome data **(Figure S1).** To our knowledge, this is the first study that investigated the quantitative effect of the interplay of host enzymes, transporters, and the gut microbiome on irinotecan tissue-specific disposition. Irinotecan hydrolysis to SN-38 was significantly higher in the intestine as compared to the liver **(Figure 1),** which corroborates with the higher intestinal abundance of CES2, the primary hydrolytic enzyme involved in SN-38 formation (Basit *et al.*, 2020). Irinotecan hydrolysis to SN-38 was limited in the liver due to poor hepatic abundance of CES2. Unlike previous studies, (Iyer *et al.*, 2002; Liu *et al.*, 2008; Palomaki *et al.*, 2009) where UGT1A1 was considered the major contributor to SN-38-G formation, our data suggest that UGT1A9 also plays a significant role in this process in the liver and kidney. Nevertheless, UGT1A1 is considered as the most important enzyme for SN-38 glucuronidation clinically that is confirmed by genetic polymorphism studies and leads to the dose reduction recommendations by the FDA for the carriers of UGT1A1*28 (Innocenti *et al.*, 2014; Palomaki *et al.*, 2009; Liu *et al.*, 2008). The genetic polymorphisms in UGT1A9 leading to an increased (UGT1A9*22) or decreased (UGT1A9 −118 (dT)9/9) activity tended to show an associated with a decreased (Carlini *et al.*, 2005) or increased GI-toxicity (Inoue *et al.*, 2013) of irinotecan, respectively, however, the clinical data are inconclusive. P-gp, BCRP, MRP2 MRP3, OATP1B1, and OATP2B1 are involved in the transport of irinotecan and its metabolites (Nakatomi *et al.*, 2001; Lalloo *et al.*, 2004; Nozawa *et al.*, 2005; Fujita *et*

DMD Fast Forward. Published on June 1, 2021 as DOI: 10.1124/dmd.121.000476
This article has not been copyedited and formatted. The final version may differ from this version.

al., 2016). However, based on our protein abundance data, P-gp and BCRP are the major contributors in the transport of irinotecan and its metabolites. This corroborates with a significantly higher exposure of irinotecan and SN-38 observed in patients with P-gp polymorphism, 1236C > T (Zhou *et al.*, 2005). Similarly, the accumulation of SN-38 and SN-38-G has been observed in the carriers of BCRP-Q141K allele (de Jong *et al.*, 2004). The role of MRP3 in SN-38-G transport was identified for the first time **(Figure 6A)**. The latter explains higher plasma and urine levels of SN-38-G after its basolateral efflux from the enterocyte and the hepatocytes into the blood (Chen *et al.*, 2012). We also identified that OATP1B1 actively transports SN-38-G into the liver, which further allows more intestinal SN-38 reactivation through biliary secretion and hydrolysis of SN-38-G **(Figure 6A)**. Such, the recovery of SN-38-G in urine (Slatter *et al.*, 2000) is likely as a result of MRP3 mediated basolateral efflux from the liver and enterocytes along with UGT1A9 mediated SN-38-G formation in the kidney. SN-38 was identified to be a substrate of both OATP1B1 and OATP2B1, but not of the basolateral efflux transporters. This explains the higher hepatic uptake and intestinal exposure of SN-38 and its ultimate excretion into the feces. Although both OATP1B1 and OATP2B1 are expressed in the liver, only OATP2B1 is expressed in the intestine (Li *et al.*, 2020). Therefore, OATP2B1 likely contributes to SN-38 re-uptake from the gut lumen in addition to the passive diffusion **(Figure 6A)**. SN-38 is indicated to be a moderate substrate of OATP1B3 (Yamaguchi *et al.*, 2008)**,** however, since OATP1B3 expression is ~4-fold lower than OATP1B1 in the liver (Prasad *et al.*, 2014) and it is not expressed in the intestine, we concluded that the role of OATP1B3 in the enterohepatic irinotecan disposition is limited. Therefore, we did not include OATP1B3 in this study. The tissue proteomics data suggest that CES mediated hydrolysis of irinotecan is the rate-limiting process in the liver, whereas SN-38 glucuronidation by UGT1A1 and its transport by intestinal and hepatic P-gp in the intestine allows greater intestinal exposure of SN-38. Intestinal P-gp, on the other hand, facilitates detoxification of the enterocytes. These data were confirmed by sequential irinotecan metabolism, which clearly demonstrated that hepatic SN-38-G formation in the liver is higher than CES mediated SN-38 formation.

DMD Fast Forward. Published on June 1, 2021 as DOI: 10.1124/dmd.121.000476
This article has not been copyedited and formatted. The final version may differ from this version.

Contrarily, the higher SN-38 formation was estimated in the intestinal S9 because of the high CES2 activity in the intestine than the liver. Similarly, the unmetabolized amount of irinotecan in the liver S9 was higher than the intestinal S9 (**Figure S4)**. Taken together, our data suggest poor elimination of SN-38-G in feces than the urine, whereas irinotecan and SN-38 were majorly eliminated into feces than the urine due to higher tissue exposure level consistent with the data from a reported mass-balance study (Mathijssen *et al.*, 2004). Since metabolism and transport mechanisms are susceptible to inter-individual variability (Turner *et al.*, 2015), quantitative assessment of the role of individual mechanisms will allow explanation of variable irinotecan disposition and toxicity caused by factors such as drug-drug interactions, genotype, sex, age, and disease conditions. Consistent with our data, several clinical drug-drug interactions and pharmacogenomic studies have confirmed the role of UGT1A1 and P-gp in irinotecan disposition and toxicity. For example, methimazole, a non-selective UGT inhibitor, significantly increased SN-38 exposure when co-administered with irinotecan (van der Bol *et al.*, 2011). Similarly, paclitaxel and cyclosporine have been shown to increase AUC or decrease clearance of SN-38 likely due to P-gp and UGT1A1 inhibition in liver and kidney, whereas, phenobarbital increases irinotecan clearance (27%) and reduces SN-38 AUC (75%) likely due to UGT induction (Innocenti *et al.*, 2004; Asai *et al.*, 2006).

In addition to the host disposition mechanisms, we confirmed that the higher SN-38 concentration in the intestine can be further nourished by β-d-glucuronidases leading to the higher exposure of the toxic metabolite as shown previously (Pellock *et al.*, 2018; Bhatt *et al.*, 2020). However, due to wide inter-individual variability in gut-microbiota composition and difficulties in quantification, β-d-glucuronidases activity rate (SN-38 reactivation from SN-38-G) was not incorporated into the tissue exposure estimation. Nevertheless, these results explain poor detection of SN-38-G in feces. These data taken together with the intestinal OATP2B1 uptake, P-gp and BCRP efflux, and high CES2 metabolism in the enterocytes, confirmed that intestinal toxicity is a contribution of multiple competing factors such as i)

DMD Fast Forward. Published on June 1, 2021 as DOI: 10.1124/dmd.121.000476
This article has not been copyedited and formatted. The final version may differ from this version.

passive diffusion of irinotecan and SN-38 into enterocytes, ii) formation and biliary or intestinal apical active efflux of SN-38 and iii) SN-38-G de-glucuronidation in the lumen by the gut microbiome. Apart from diarrhea, other toxicities of irinotecan such as neutropenia and myelosuppression have been observed in clinic, but the mechanisms are still unclear (Liu *et al.*, 2008). However, the high expression of CES2 in bone marrow compared to CES1 and the absence of UGTs (Uhlén *et al.*, 2015) suggest that irinotecan hydrolysis is the likely cause of the toxicity. A detailed characterisation of the metabolism and transport mechanisms in bone marrow is warranted for a conclusive understanding of the toxicity mechanism.

One of the major limitations of our study was the lack of intestinal tissue concentration data to validate the proteomics-based IVIVE predictions. Once the tissue concentration data are available, a comprehensive PBPK model can be developed and validated based on the data presented here. Irinotecan and SN-38 are highly lipophobic compounds with good membrane permeability, but we did not account passive diffusion in the f_t calculation. However, passive diffusion should ideally be considered in tissue exposure estimation. Consistent with our data, biliary efflux and intestinal UGT1A1 mediated SN-38 metabolism has been proposed as a toxicity mechanism previously (Chen *et al.*, 2013).

In conclusion, this is the first study to our knowledge that integrates *in vitro* host metabolism and transport kinetics with tissue proteomics and gut microbial activation data of irinotecan and its metabolites to explain high intestinal SN-38 exposure and toxicity **(Figure 6B)**. Key processes involved in SN-38 intestinal disposition were identified that can be leveraged to reduce toxicity. Since the fractional contributions of individual mechanisms (f_m or f_t) depends on the enzyme or transporter abundance, the inter-tissue or interindividual variability of irinotecan can be predicted by integrating the quantitative proteomics data with the in vitro intrinsic clearance data from this study along with other parameters (e.g., protein binding and blood flow to organs) using a PBPK model in the future. This approach can be extended to cancer cells to stratify responders and non-responders based on intracellular SN-38

DMD Fast Forward. Published on June 1, 2021 as DOI: 10.1124/dmd.121.000476
This article has not been copyedited and formatted. The final version may differ from this version.

formation. Finally, the tissue-proteomics based quantitative model presented in this study can be applied to predict disposition and response of drugs undergoing complex metabolism, transport, and enterohepatic recycling such as statins, telmisartan, digoxin, and lamotrigine, Such tissue proteomics-informed drug disposition study is important for safe and cost-effective clinical trial design during drug development and reduce drug attrition due to unpredictable efficacy and safety outcomes.

DMD Fast Forward. Published on June 1, 2021 as DOI: 10.1124/dmd.121.000476
This article has not been copyedited and formatted. The final version may differ from this version.

ACKNOWLEDGEMENT

Authors would like to thank Solvo Biotechnology and BioIVT Inc for providing cell lines, membrane vesicles and human hepatocytes used in this study.

DMD Fast Forward. Published on June 1, 2021 as DOI: 10.1124/dmd.121.000476
This article has not been copyedited and formatted. The final version may differ from this version.

AUTHORSHIP CONTRIBUTIONS

Participated in research design: Parvez, Basit, Jariwala, Redinbo, Prasad

Conducted experiments: Parvez, Basit, Jariwala

Contributed new reagents or analytic tools: Gáborik, Kis, Heyward

Performed data analysis: Parvez, Basit, Jariwala, Redinbo, Prasad

Wrote or contributed to the writing of the manuscript: Parvez, Basit, Jariwala, Gáborik, Kis, Heyward, Redinbo, Prasad

DMD Fast Forward. Published on June 1, 2021 as DOI: 10.1124/dmd.121.000476
This article has not been copyedited and formatted. The final version may differ from this version.

References

Ando Y, Saka H, Ando M, Sawa T, Muro K, Ueoka H, Yokoyama A, Saitoh S, Shimokata K, and Hasegawa Y (2000) Polymorphisms of UDP-glucuronosyltransferase gene and irinotecan toxicity: a pharmacogenetic analysis. *Cancer Res* **60**:6921–6926, United States.

Asai G, Yamamoto N, Kurata T, Tamura K, Uejima H, Nakagawa K, and Fukuoka M (2006) Phase I and pharmacokinetic study of combination chemotherapy using irinotecan and paclitaxel in patients with lung cancer. *J Thorac Oncol Off Publ Int Assoc Study Lung Cancer* **1**:226–230, United States.

Basit A, Neradugomma NK, Wolford C, Fan PW, Murray B, Takahashi RH, Khojasteh SC, Smith BJ, Heyward S, Totah RA, Kelly EJ, and Prasad B (2020) Characterization of Differential Tissue Abundance of Major Non-CYP Enzymes in Human. *Mol Pharm* **17**:4114–4124, American Chemical Society.

Best BM, Letendre SL, Brigid E, Clifford DB, Collier AC, Gelman BB, McArthur JC, McCutchan JA, Simpson DM, Ellis R, Capparelli E V, and Grant I (2009) Low atazanavir concentrations in cerebrospinal fluid. *AIDS* **23**:83–87.

Bhatt AP, Pellock SJ, Biernat KA, Walton WG, Wallace BD, Creekmore BC, Letertre MM, Swann JR, Wilson ID, Roques JR, Darr DB, Bailey ST, Montgomery SA, Roach JM, Azcarate-Peril MA, Sartor RB, Gharaibeh RZ, Bultman SJ, and Redinbo MR (2020) Targeted inhibition of gut bacterial β-glucuronidase activity enhances anticancer drug efficacy. *Proc Natl Acad Sci* **117**:7374 LP – 7381.

Bhatt S, Northcott C, Wisialowski T, Li D, and Steidl-Nichols J (2019) Preclinical to Clinical Translation of Hemodynamic Effects in Cardiovascular Safety Pharmacology Studies. *Toxicol Sci* **169**:272–279, United States.

Carlini LE, Meropol NJ, Bever J, Andria ML, Hill T, Gold P, Rogatko A, Wang H, and

Blanchard RL (2005) UGT1A7 and UGT1A9 Polymorphisms Predict Response and Toxicity in Colorectal Cancer Patients Treated with Capecitabine/Irinotecan. *Clin Cancer Res* **11**:1226 LP – 1236.

Chen S, Yueh M-F, Bigo C, Barbier O, Wang K, Karin M, Nguyen N, and Tukey RH (2013) Intestinal glucuronidation protects against chemotherapy-induced toxicity by irinotecan (CPT-11). *Proc Natl Acad Sci U S A* **110**:19143–19148, National Academy of Sciences.

Chen X, Peer CJ, Alfaro R, Tian T, Spencer SD, and Figg WD (2012) Quantification of irinotecan, SN38, and SN38G in human and porcine plasma by ultra high-performance liquid chromatography-tandem mass spectrometry and its application to hepatic chemoembolization. *J Pharm Biomed Anal* **62**:140–148.

de Jong FA, Marsh S, Mathijssen RHJ, King C, Verweij J, Sparreboom A, and McLeod HL (2004) ABCG2 pharmacogenetics: ethnic differences in allele frequency and assessment of influence on irinotecan disposition. *Clin cancer Res an Off J Am Assoc Cancer Res* **10**:5889–5894, United States.

Di L (2019) The Impact of Carboxylesterases in Drug Metabolism and Pharmacokinetics. *Curr Drug Metab* **20**:91–102.

Di Martino MT, Arbitrio M, Leone E, Guzzi PH, Rotundo MS, Ciliberto D, Tomaino V, Fabiani F, Talarico D, Sperlongano P, Doldo P, Cannataro M, Caraglia M, Tassone P, and Tagliaferri P (2011) Single nucleotide polymorphisms of ABCC5 and ABCG1 transporter genes correlate to irinotecan-associated gastrointestinal toxicity in colorectal cancer patients: a DMET microarray profiling study. *Cancer Biol Ther* **12**:780–787, United States.

Fujita D, Saito Y, Nakanishi T, and Tamai I (2016) Organic Anion Transporting Polypeptide (OATP)2B1 Contributes to Gastrointestinal Toxicity of Anticancer Drug SN-38, Active Metabolite of Irinotecan Hydrochloride. *Drug Metab Dispos* **44**:1–7, United States.

Fujiyama N, Miura M, Kato S, Sone T, Isobe M, and Satoh S (2010) Involvement of Carboxylesterase 1 and 2 in the Hydrolysis of Mycophenolate Mofetil. *Drug Metab Dispos* **38**:2210 LP – 2217.

Gibson RJ, and Keefe DMK (2006) Cancer chemotherapy-induced diarrhoea and constipation: mechanisms of damage and prevention strategies. *Support care cancer Off J Multinatl Assoc Support Care Cancer* **14**:890–900, Germany.

Gilbert DC, Chalmers AJ, and El-Khamisy SF (2012) Topoisomerase I inhibition in colorectal cancer: biomarkers and therapeutic targets. *Br J Cancer* **106**:18–24, Nature Publishing Group.

Guo Y, Chu X, Parrott NJ, Brouwer KLR, Hsu V, Nagar S, Matsson P, Sharma P, Snoeys J, Sugiyama Y, Tatosian D, Unadkat JD, Huang S-M, and Galetin A (2018) Advancing Predictions of Tissue and Intracellular Drug Concentrations Using In Vitro, Imaging and Physiologically Based Pharmacokinetic Modeling Approaches. *Clin Pharmacol Ther* **104**:865–889.

Hageman MJ, and Morozowich W (2007) Case Study: Irinotecan (CPT-11), A Water-soluble Prodrug of SN-38 BT - Prodrugs: Challenges and Rewards Part 1, in (Stella VJ, Borchardt RT, Hageman Michael J, Oliyai R, Maag H, and Tilley JW eds) pp 1269–1279, Springer New York, New York, NY.

Hanioka N, Ozawa S, Jinno H, Ando M, Saito Y, and Sawada J (2001) Human liver UDP-glucuronosyltransferase isoforms involved in the glucuronidation of 7-ethyl-10-hydroxycamptothecin. *Xenobiotica* **31**:687–699, England.

Hay M, Thomas DW, Craighead JL, Economides C, and Rosenthal J (2014) Clinical development success rates for investigational drugs. *Nat Biotechnol* **32**:40–51, United States.

Humerickhouse R, Lohrbach K, Li L, Bosron WF, and Dolan ME (2000) Characterization of

CPT-11 hydrolysis by human liver carboxylesterase isoforms hCE-1 and hCE-2. *Cancer Res* **60**:1189–1192, United States.

Innocenti F, Schilsky RL, Ramírez J, Janisch L, Undevia S, House LK, Das S, Wu K, Turcich M, Marsh R, Karrison T, Maitland ML, Salgia R, and Ratain MJ (2014) Dose-finding and pharmacokinetic study to optimize the dosing of irinotecan according to the UGT1A1 genotype of patients with cancer. *J Clin Oncol Off J Am Soc Clin Oncol* **32**:2328–2334.

Innocenti F, Undevia SD, Ramírez J, Mani S, Schilsky RL, Vogelzang NJ, Prado M, and Ratain MJ (2004) A phase I trial of pharmacologic modulation of irinotecan with cyclosporine and phenobarbital. *Clin Pharmacol Ther* **76**:490–502, United States.

Inoue K, Sonobe M, Kawamura Y, Etoh T, Takagi M, Matsumura T, Kikuyama M, Kimura M, Minami S, Utsuki H, Yamazaki T, Suzuki T, Tsuji D, Hayashi H, and Itoh K (2013) Polymorphisms of the UDP-Glucuronosyl Transferase 1A Genes Are Associated with Adverse Events in Cancer Patients Receiving Irinotecan-Based Chemotherapy. *Tohoku J Exp Med* **229**:107–114.

Iyer L, Das S, Janisch L, Wen M, Ramírez J, Karrison T, Fleming GF, Vokes EE, Schilsky RL, and Ratain MJ (2002) UGT1A1*28 polymorphism as a determinant of irinotecan disposition and toxicity. *Pharmacogenomics J* **2**:43–47.

Izumi S, Nozaki Y, Maeda K, Komori T, Takenaka O, Kusuhara H, and Sugiyama Y (2015) Investigation of the impact of substrate selection on in vitro organic anion transporting polypeptide 1B1 inhibition profiles for the prediction of drug-drug interactions. *Drug Metab Dispos* **43**:235–247.

Jariwala PB, Pellock SJ, Goldfarb D, Cloer EW, Artola M, Simpson JB, Bhatt AP, Walton WG, Roberts LR, Major MB, Davies GJ, Overkleeft HS, and Redinbo MR (2020) Discovering the Microbial Enzymes Driving Drug Toxicity with Activity-Based Protein Profiling. *ACS Chem Biol* **15**:217–225, American Chemical Society.

Jinno H, Tanaka-Kagawa T, Hanioka N, Saeki M, Ishida S, Nishimura T, Ando M, Saito Y, Ozawa S, and Sawada J-I (2003) Glucuronidation of 7-ethyl-10-hydroxycamptothecin (SN-38), an active metabolite of irinotecan (CPT-11), by human UGT1A1 variants, G71R, P229Q, and Y486D. *Drug Metab Dispos* **31**:108–113, United States.

Kola I, and Landis J (2004) Can the pharmaceutical industry reduce attrition rates?, England.

Lalloo AK, Luo FR, Guo A, Paranjpe P V, Lee S-H, Vyas V, Rubin E, and Sinko PJ (2004) Membrane transport of camptothecin: facilitation by human P-glycoprotein (ABCB1) and multidrug resistance protein 2 (ABCC2). *BMC Med* **2**:16.

Lau YY, Sapidou E, Cui X, White RE, and Cheng K-C (2002) Development of a novel in vitro model to predict hepatic clearance using fresh, cryopreserved, and sandwich-cultured hepatocytes. *Drug Metab Dispos* **30**:1446–1454, United States.

Li CY, Basit A, Gupta A, Gaborik Z, Kis E, and Prasad B (2019) Major glucuronide metabolites of testosterone are primarily transported by MRP2 and MRP3 in human liver, intestine and kidney. *J Steroid Biochem Mol Biol* **191**:105350, England.

Li CY, Gupta A, Gáborik Z, Kis E, and Prasad B (2020) OATP-mediated hepatic uptake of glucuronide metabolites of androgens. *Mol Pharmacol* mol.120.119891.

Li H, He J, and Jia W (2016) The influence of gut microbiota on drug metabolism and toxicity. *Expert Opin Drug Metab Toxicol* **12**:31–40.

Liu C-Y, Chen P-M, Chiou T-J, Liu J-H, Lin J-K, Lin T-C, Chen W-S, Jiang J-K, Wang H-S, and Wang W-S (2008) UGT1A1*28 polymorphism predicts irinotecan-induced severe toxicities without affecting treatment outcome and survival in patients with metastatic colorectal carcinoma. *Cancer* **112**:1932–1940, United States.

Mateus A, Gordon LJ, Wayne GJ, Almqvist H, Axelsson H, Seashore-Ludlow B, Treyer A, Matsson P, Lundbäck T, West A, Hann MM, and Artursson P (2017) Prediction of intracellular exposure bridges the gap between target- and cell-based drug discovery.

Proc Natl Acad Sci **114**:E6231 LP-E6239.

Mathijssen RHJ, de Jong FA, van Schaik RHN, Lepper ER, Friberg LE, Rietveld T, de Bruijn P, Graveland WJ, Figg WD, Verweij J, and Sparreboom A (2004) Prediction of irinotecan pharmacokinetics by use of cytochrome P450 3A4 phenotyping probes. *J Natl Cancer Inst* **96**:1585–1592, United States.

Nakatomi K, Yoshikawa M, Oka M, Ikegami Y, Hayasaka S, Sano K, Shiozawa K, Kawabata S, Soda H, Ishikawa T, Tanabe S, and Kohno S (2001) Transport of 7-ethyl-10-hydroxycamptothecin (SN-38) by breast cancer resistance protein ABCG2 in human lung cancer cells. *Biochem Biophys Res Commun* **288**:827–832, United States.

Nozawa T, Minami H, Sugiura S, Tsuji A, and Tamai I (2005) Role of organic anion transporter OATP1B1 (OATP-C) in hepatic uptake of irinotecan and its active metabolite, 7-ethyl-10-hydroxycamptothecin: in vitro evidence and effect of single nucleotide polymorphisms. *Drug Metab Dispos* **33**:434–439, United States.

Palomaki GE, Bradley LA, Douglas MP, Kolor K, and Dotson WD (2009) Can UGT1A1 genotyping reduce morbidity and mortality in patients with metastatic colorectal cancer treated with irinotecan? An evidence-based review. *Genet Med* **11**:21–34.

Pellock SJ, Creekmore BC, Walton WG, Mehta N, Biernat KA, Cesmat AP, Ariyarathna Y, Dunn ZD, Li B, Jin J, James LI, and Redinbo MR (2018) Gut Microbial β-Glucuronidase Inhibition via Catalytic Cycle Interception. , doi: 10.1021/acscentsci.8b00239.s001.

Pommier Y (2006) Topoisomerase I inhibitors: camptothecins and beyond. *Nat Rev Cancer* **6**:789–802, England.

Prasad B, Evers R, Gupta A, Hop CECA, Salphati L, Shukla S, Ambudkar S V, and Unadkat JD (2014) Interindividual variability in hepatic organic anion-transporting polypeptides and P-glycoprotein (ABCB1) protein expression: quantification by liquid chromatography tandem mass spectroscopy and influence of genotype, age, and sex.

Drug Metab Dispos **42**:78–88.

Rivory LP, and Robert J (1995) Molecular, cellular, and clinical aspects of the pharmacology of 20(S)camptothecin and its derivatives. *Pharmacol Ther* **68**:269–296, England.

Sharma A, Buschmann MM, and Gilbert JA (2019) Pharmacomicrobiomics: The Holy Grail to Variability in Drug Response? *Clin Pharmacol Ther* **106**:317–328, United States.

Slatter JG, Schaaf LJ, Sams JP, Feenstra KL, Johnson MG, Bombardt PA, Cathcart KS, Verburg MT, Pearson LK, Compton LD, Miller LL, Baker DS, Pesheck C V, and Lord RS 3rd (2000) Pharmacokinetics, metabolism, and excretion of irinotecan (CPT-11) following I.V. infusion of [(14)C]CPT-11 in cancer patients. *Drug Metab Dispos* **28**:423–433, United States.

Sliwoski G, Kothiwale S, Meiler J, and Lowe Jr EW (2013) Computational methods in drug discovery. *Pharmacol Rev* **66**:334–395, The American Society for Pharmacology and Experimental Therapeutics.

Sun C, Chen L, and Shen Z (2019) Mechanisms of gastrointestinal microflora on drug metabolism in clinical practice. *Saudi Pharm J SPJ Off Publ Saudi Pharm Soc* **27**:1146–1156, Elsevier.

Teft WA, Welch S, Lenehan J, Parfitt J, Choi Y-H, Winquist E, and Kim RB (2015) OATP1B1 and tumour OATP1B3 modulate exposure, toxicity, and survival after irinotecan-based chemotherapy. *Br J Cancer* **112**:857–865, Nature Publishing Group.

Tovar-y-Romo LB, Bumpus NN, Pomerantz D, Avery LB, Sacktor N, McArthur JC, and Haughey NJ (2012) Dendritic spine injury induced by the 8-hydroxy metabolite of efavirenz. *J Pharmacol Exp Ther* **343**:696–703.

Turner RM, Park BK, and Pirmohamed M (2015) Parsing interindividual drug variability: an emerging role for systems pharmacology. *Wiley Interdiscip Rev Syst Biol Med* **7**:221–241, John Wiley & Sons, Inc.

Uhlén M, Fagerberg L, Hallström BM, Lindskog C, Oksvold P, Mardinoglu A, Sivertsson Å, Kampf C, Sjöstedt E, Asplund A, Olsson I, Edlund K, Lundberg E, Navani S, Szigyarto CA-K, Odeberg J, Djureinovic D, Takanen JO, Hober S, Alm T, Edqvist P-H, Berling H, Tegel H, Mulder J, Rockberg J, Nilsson P, Schwenk JM, Hamsten M, von Feilitzen K, Forsberg M, Persson L, Johansson F, Zwahlen M, von Heijne G, Nielsen J, and Pontén F (2015) Proteomics. Tissue-based map of the human proteome. *Science* **347**:1260419, United States.

van der Bol JM, Visser TJ, Loos WJ, de Jong FA, Wiemer EAC, van Aken MO, Planting AS, Schellens JH, Verweij J, and Mathijssen RHJ (2011) Effects of methimazole on the elimination of irinotecan. *Cancer Chemother Pharmacol* **67**:231–236.

Waring MJ, Arrowsmith J, Leach AR, Leeson PD, Mandrell S, Owen RM, Pairaudeau G, Pennie WD, Pickett SD, Wang J, Wallace O, and Weir A (2015) An analysis of the attrition of drug candidates from four major pharmaceutical companies. *Nat Rev Drug Discov* **14**:475–486.

Xu M, Bhatt DK, Yeung CK, Claw KG, Chaudhry AS, Gaedigk A, Pearce RE, Broeckel U, Gaedigk R, Nickerson DA, Schuetz E, Rettie AE, Leeder JS, Thummel KE, and Prasad B (2017) Genetic and Nongenetic Factors Associated with Protein Abundance of Flavin-Containing Monooxygenase 3 in Human Liver. *J Pharmacol Exp Ther* **363**:265–274, United States.

Yamaguchi H, Kobayashi M, Okada M, Takeuchi T, Unno M, Abe T, Goto J, Hishinuma T, and Mano N (2008) Rapid screening of antineoplastic candidates for the human organic anion transporter OATP1B3 substrates using fluorescent probes. *Cancer Lett* **260**:163–169.

Zhang H, Basit A, Busch D, Yabut K, Bhatt DK, Drozdzik M, Ostrowski M, Li A, Collins C, Oswald S, and Prasad B (2018) Quantitative characterization of UDP-glucuronosyltransferase 2B17 in human liver and intestine and its role in testosterone

first-pass metabolism. *Biochem Pharmacol* **156**:32–42, England.

Zhang X, Wang R, Piotrowski M, Zhang H, and Leach KL (2015) Intracellular concentrations determine the cytotoxicity of adefovir, cidofovir and tenofovir. *Toxicol In Vitro* **29**:251–258, England.

Zhou Q, Sparreboom A, Tan E-H, Cheung Y-B, Lee A, Poon D, Lee EJD, and Chowbay B (2005) Pharmacogenetic profiling across the irinotecan pathway in Asian patients with cancer. *Br J Clin Pharmacol* **59**:415–424, Blackwell Science Inc.

DMD Fast Forward. Published on June 1, 2021 as DOI: 10.1124/dmd.121.000476
This article has not been copyedited and formatted. The final version may differ from this version.

FOOTNOTE

This work was supported by Eunice Kennedy Shriver National Institute of Child Health and Human Development, NIH grant (R01.HD081299) and the Department of Pharmaceutical Sciences, Washington State University, Spokane, WA.

The authors have no financial disclosers to make.

DMD Fast Forward. Published on June 1, 2021 as DOI: 10.1124/dmd.121.000476
This article has not been copyedited and formatted. The final version may differ from this version.

FIGURE CAPTION

Figure 1. Mechanisms of irinotecan and SN-38 metabolism.

Figure 2. Metabolism of irinotecan in human liver and intestine S9 fractions, and human hepatocytes.

Figure 3. In vitro uptake and efflux transport kinetics of irinotecan, SN-38, and SN-38-G.

Figure 4. Fractional contributions of individual enzymes (f_m) and transporters (f_t) to the clearance of irinotecan, SN-38, and SN-38-G in different tissues.

Figure 5. Re-activation of SN-38 from SN-38-G by bacterial β-glucuronidase.

Figure 6. Tissue distribution and mechanistic disposition mechanism of irinotecan, SN-38 and SN-38-G.

DMD Fast Forward. Published on June 1, 2021 as DOI: 10.1124/dmd.121.000476
This article has not been copyedited and formatted. The final version may differ from this version.

FIGURE LEGENDS

Figure 1. Mechanisms of irinotecan and SN-38 metabolism. Sequential metabolism scheme of irinotecan by CES and UGT enzymes (A). Concentration-dependent SN-38 formation (B) and SN-38-G formation (C) by CESs and UGTs, respectively. The kinetic parameters (K_m and V_{max}) were determined using non-linear regression model (Michaelis-Menten) in GraphPad prism (V 5.1). Data represent the mean ± SD of triplicate experiments.

Figure 2. Metabolism of irinotecan in human liver and intestine S9 fractions, and human hepatocytes. Concentration-dependent sequential metabolite formation rates of SN-38 from irinotecan (1 - 400 µM) (A) SN-38-G from SN-38 (1 - 120 µM) (B) in the liver and intestinal S9 fractions. The ratio of SN-38 and SN-38-G formation rates in the sequential metabolism in the liver and the intestinal S9 showed significant tissue specific differences in the UGT and CES activities (C). Direct conversion of SN-38 to SN-38-G by UGT in the liver and the intestine S9 fractions showed higher activity in the liver (D). These data were reproduced in human hepatocyte experiment (E-G), where the ratio of SN-38 to irinotecan represents CES activity (E) and SN-38-G to SN-38 represents UGT activity (F). The total metabolites (SN-38 plus SN-38-G) to irinotecan ratio represents the interplay between CES and UGT activity (G). Data represent the mean ± SD of triplicate experiments. Significant differences between the hepatocytes lots (n=3) are indicated (***, p = 0.001).

Figure 3. In vitro uptake and efflux transport kinetics of irinotecan, SN-38, and SN-38-G. Concentration-dependent net transport of irinotecan (A), SN-38 (B), and SN-38-G (C). The net transport rates are expressed after normalization with the transporter protein abundance (pmol/mg of vesicular membrane protein). SN-38 net uptake by OATP1B1 (D), OATP2B1 (E) and SN-38-G by OATP1B1 (F). Mock transfected vesicles or cells were used as the negative controls and the transport rate was subtracted to estimate the net transporter

DMD Fast Forward. Published on June 1, 2021 as DOI: 10.1124/dmd.121.000476
This article has not been copyedited and formatted. The final version may differ from this version.

mediated uptake. Transport kinetics parameters (K_m and V_{max}) were estimated using non-linear regression model (Michaelis-Menten) in GraphPad prism (V 5.1). Data represent the mean ± SD of triplicate experiments.

Figure 4. Fractional contributions of individual enzymes (f_m) and transporters (f_t) to the clearance of irinotecan, SN-38, and SN-38-G in different tissues. Data represents the extrapolated and normalized fractional metabolism of each enzymes in human liver, intestine, kidney, heart, and lung (A and B). The fractional efflux transport (f_t) for irinotecan (C), SN-38 (D), and SN-38-G (E), and f_t for uptake transport of SN-38 (F) after scaling by the tissue proteomics data (pmol/ tissue).

Figure 5. Re-activation of SN-38 from SN-38-G by bacterial β-glucuronidase. The reactivation rate was determined by incubating SN-38-G with the human fecal extracts (n=7; 3 males and 3 females) (A). The bacterial β-glucuronidase enzyme abundance (LFQ intensity) showed good correlation with the SN38-G activation rate (B).

Figure 6. Tissue distribution and mechanistic disposition mechanism of irinotecan, SN-38 and SN-38-G. Major metabolites and the corresponding enzymes/transporters are marked in bold (A). SN-38 and SN-38-G formation rates (%) in the liver and the intestine (B).

DMD Fast Forward. Published on June 1, 2021 as DOI: 10.1124/dmd.121.000476
This article has not been copyedited and formatted. The final version may differ from this version.

Table 1. Metabolism and transport kinetics parameters of irinotecan, SN-38, and SN-38-G.

Substrate	**Enzyme/ Transporter**	**K_m, µM (95% CI)**	**V_{max}, pmol/min/mg protein (95% CI)**	**Intrinsic CL (µl/min/pmol protein)**
Irinotecan	CES1	150 (10-360)	202 (76-323)	0.0002
	CES2	351 (261-441)	2281 (1946-2615)	0.0016
SN-38	UGT1A1	18.7 (8.0-29.3)	1283 (1035-1530)	0.56
	UGT1A6	17.1 (5.2-38.5)	30.8 (18.0-43.4)	0.01
	UGT1A9	11.6 (4-23.2)	30.7 (21.5-40.0)	0.16
	UGT2B15	85.18 (0-258)	61.5 (6.0-129)	0.01
Irinotecan	P-gp	20.4 (18-23)	14676 (14117-15236)	53.20
	BCRP	31.9 (22-42)	7993 (7173-8814)	67.57
	MRP2	40.1 (29-51)	6378 (5787-6987)	2.83
SN-38	OATP1B1	267.2 (50-778)	8735 (4212-21682)	13.81
	OATP2B1	4.8 (2.5-7.0)	27.4 (24-31)	0.13
	P-gp	23.0 (19-27)	22389 (21216-23563)	72.11
	BCRP	26.5 (2-74)	17354 (1424-33285)	176.08
SN-38-G	OATP1B1	40.0 (13-67)	1011 (764-1258)	10.19
	BCRP	11.7 (3-20)	33829 (26484-41174)	775.35
	MRP2	13.62 (10-17)	8277 (7723-8832)	10.81
	MRP3	57.7 (2.3-113)	5365 (2817-7912)	0.67

Figure 1.

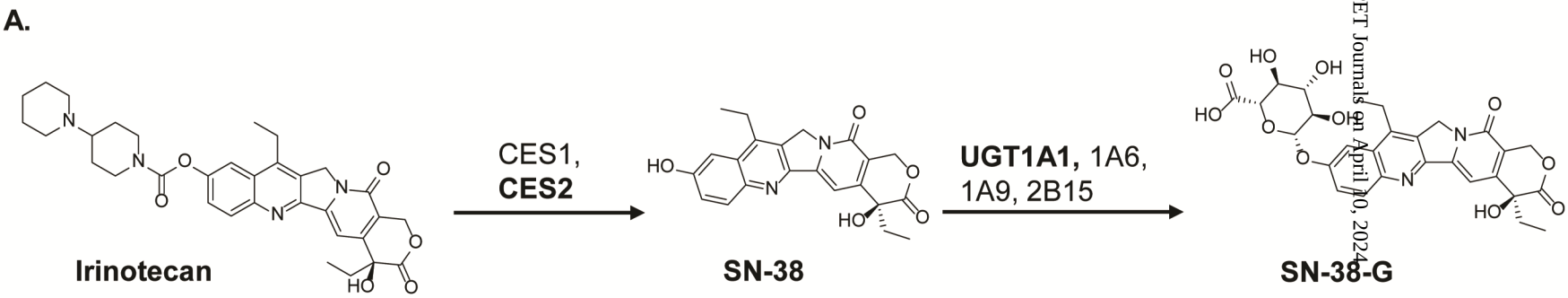

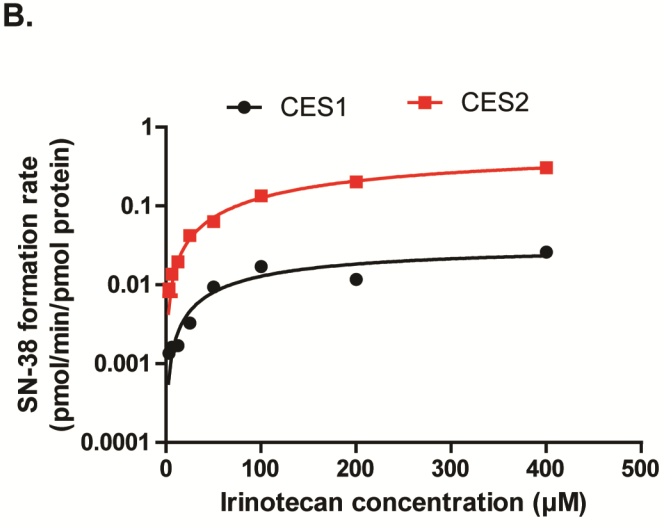

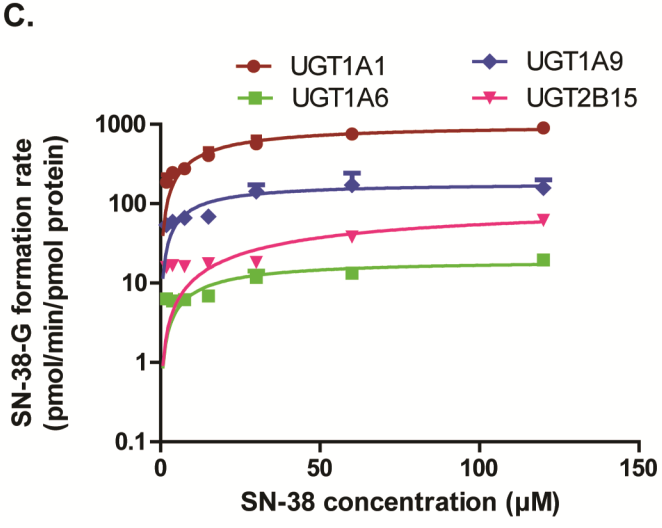

Figure 2.

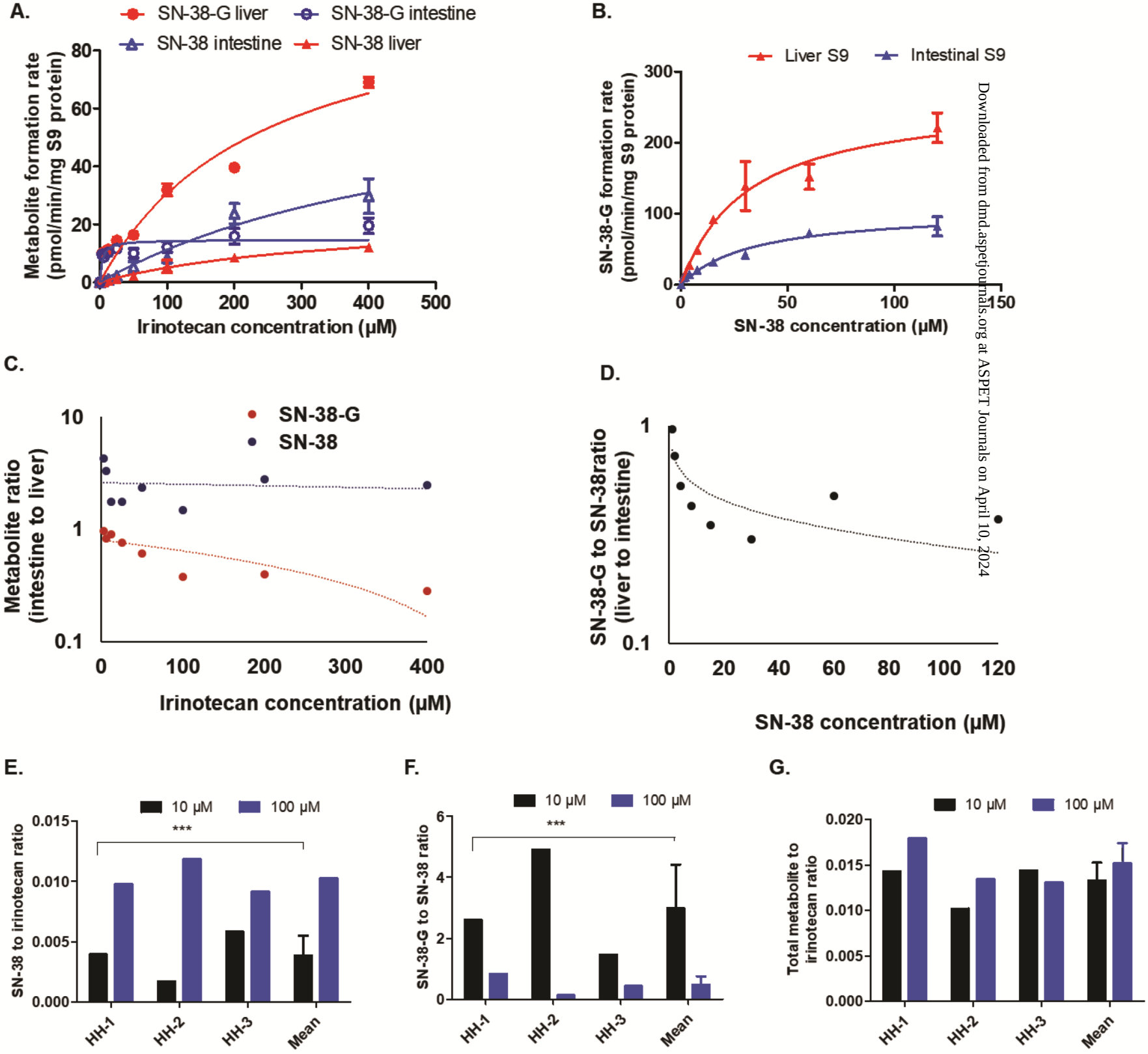

Figure 3.

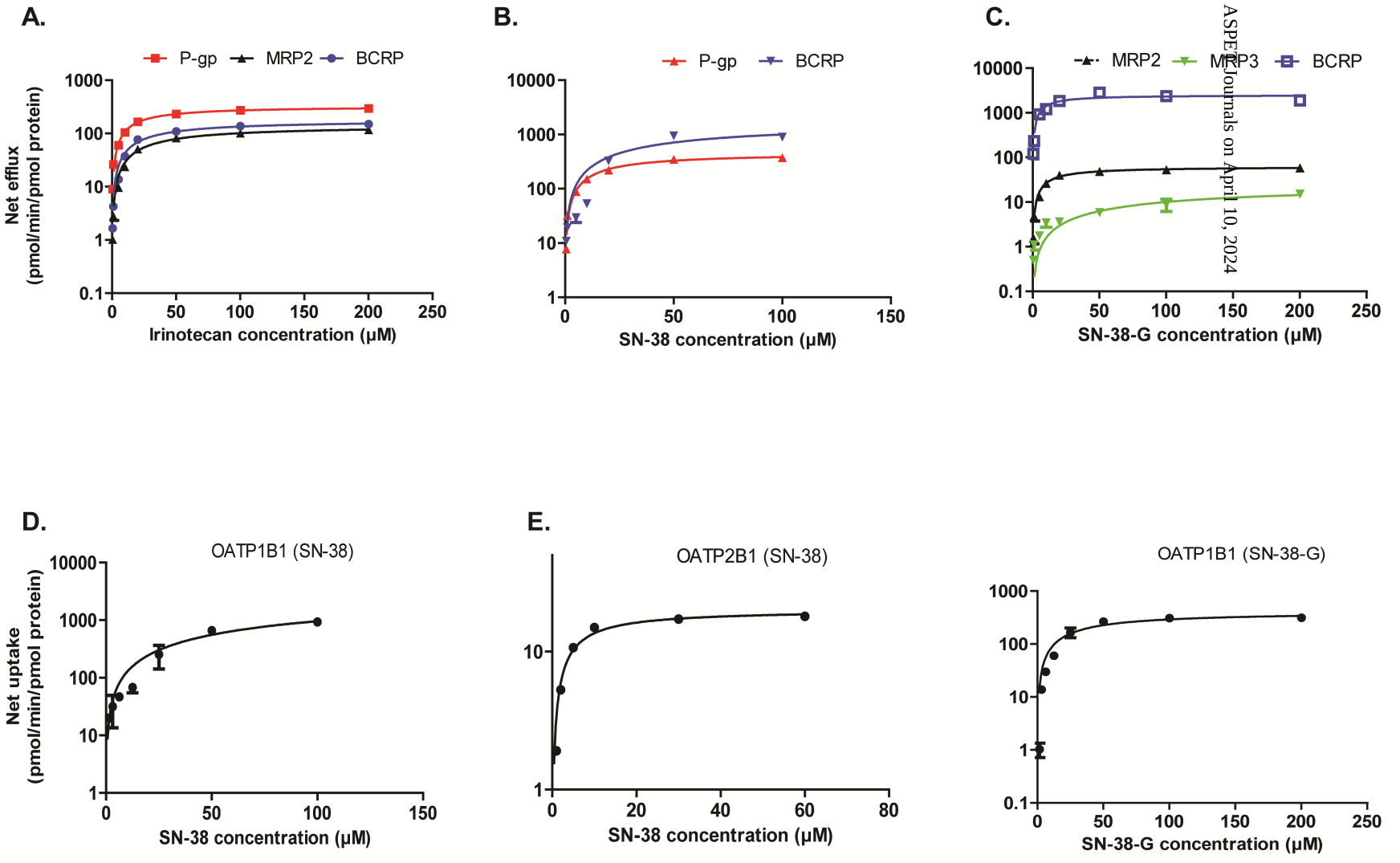

Figure 4.

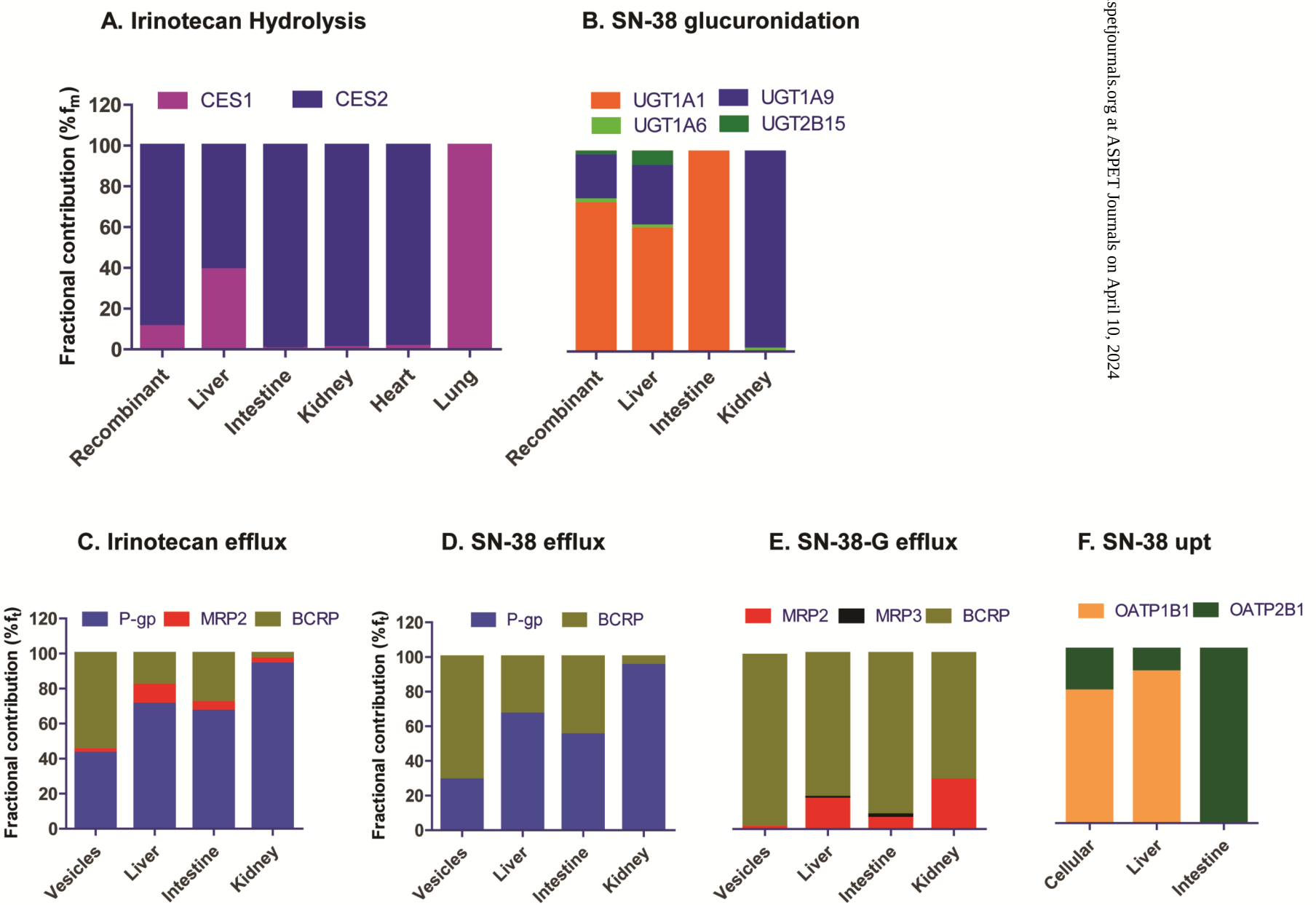

Figure 5.

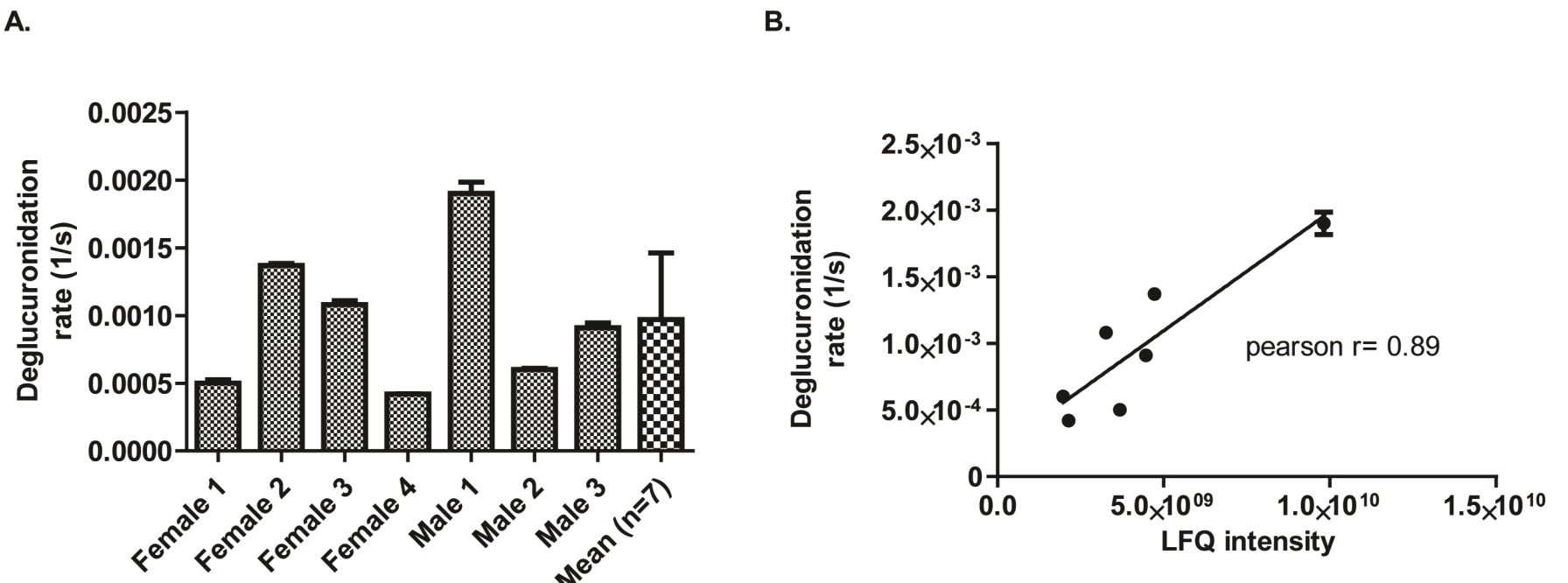

Figure 6.